PAPER

Check for updates

From symmetric to asymmetric: tuning photophysical and rectifying properties in [2.2]paracyclophanes

Karla D. Hernandez Gomora, [ID] [ab] Manikanta Makala, [ID] [bc] Evan J. Kumar, [ID] [bc] Kaizhen Zhang,[ab] Philip Hadjipetkov,[ab] David Keith,[ab] Dundappa Mumbaraddi, [ID] [ab] Ajay Ram Srimath Kandada, [ID] [bc] Swathi Kadaba*[bd] and Cedric Schaack [ID] *[ab]

[2.2]Paracyclophane (PCP) scaffolds, with their rigid, non-planar geometries and through-space π-conjugation, offer a unique platform for the development of advanced optoelectronic materials. In this study, we synthesize and characterize a series of racemic PCP derivatives bearing electron-donating (*e.g.*, −OCH₃) and electron-withdrawing (*e.g.*, −CN) substituents to explore their photophysical properties and potential as charge-transporting and rectifying materials. Solution-phase spectroscopy reveals that donor–acceptor (D–A) PCPs exhibit pronounced charge-transfer (CT) emission, with large Stokes shifts up to 166 nm, minimal spectral overlap, and solvent-dependent photoluminescence maxima shifting from 396 nm in hexanes to 474 nm in DMF. Photoluminescence quantum yields also increase substantially, from 1% in symmetrically substituted to 31% in D–A compounds. Aggregation studies reveal distinct photoluminescence modulation: D–A compounds form both J- and H-aggregates, while symmetric analogs show J-aggregation. Electrical measurements using a eutectic liquid gallium–indium (EGaIn) top contact electrode reveal that while conductance can be varied over four orders of magnitude depending on substitution pattern, D–A PCPs exhibit pronounced current rectification, achieving rectification ratios up to 200 in amorphous thin films. These findings establish functionalized PCPs as promising dual-mode materials for organic optoelectronics, capable of both environmental photoluminescence modulation and efficient molecular rectification.

Introduction

Organic π-conjugated materials with donor–acceptor (D–A) architectures are among the most widely studied molecular systems in modern materials chemistry. Their strong intramolecular charge-transfer (ICT) characteristics lead to well-defined optical transitions, tunable emission energies, and solvatochromic behavior in solution.[1–6] These features make them ideal candidates for a variety of optoelectronic applications, including sensors, photodetectors, field-effect transistors, and nonlinear optical materials (NLO).[7–10] In the solid state, D–A molecules play a central role in organic light-emitting diodes (OLEDs), where their ability to stabilize excited states and control emission pathways enables efficient radiative recombination.[11] The strategic placement of donor and acceptor units can be used to modulate singlet–triplet energy gaps, facilitate thermally activated delayed fluorescence (TADF), and control emission bandwidth.[12] However, despite the extensive exploration of their emissive properties, the potential for these same D–A materials to exhibit stimuli-responsive behavior such as modulation of emission in response to aggregation, polarity, or electric fields has recently garnered the interest of researchers.[13–15] This emerging direction holds promise for next-generation optical devices, where dynamic control over emission or conductivity is desirable.[16]

In parallel with optoelectronic advances, there is growing interest in harnessing D–A systems for molecular rectification. Organic diodes are devices that permit charge flow preferentially in one direction, forming a cornerstone of molecular electronics. Rectification in single-molecule junctions has been demonstrated with a wide range of D–A chromophores, where asymmetric electronic structures and interfacial dipoles contribute to diode-like behavior.[17–19] However, translating molecular rectification into ensemble-scale measurements remains a challenge due to issues of film morphology, contact resistance, and reproducibility.[20,21] Recent advances in eutectic

a Department of Chemistry, Wake Forest University, Winston-Salem, North Carolina 27109, USA. E-mail: schaacc@wfu.edu

b Center for Functional Materials, Wake Forest University, Winston-Salem, North Carolina 27109, USA

c Department of Physics, Wake Forest University, Winston-Salem, North Carolina 27109, USA

d Center for Nanotechnology and Quantum Materials, Department of Physics, Wake Forest University, Winston-Salem, North Carolina 27105, USA
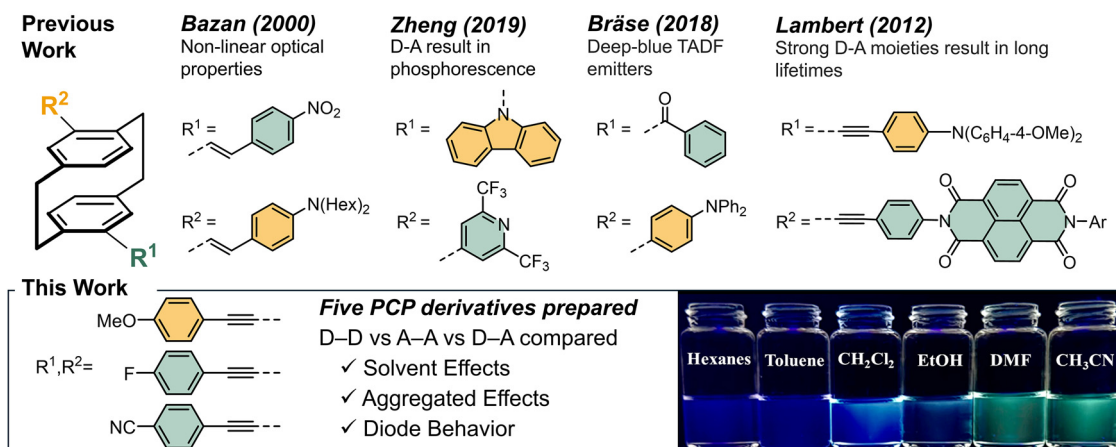
This journal is © The Royal Society of Chemistry 2025

J. Mater. Chem. C, 2025, **13**, 21759–21767 | **21759**

Fig. 1 Previous reports demonstrated valuable properties in D–A paracyclophanes, from Bazan and co-workers' NLO-active bis-styryl PCP,[38] blue emitters by Zheng and Bräse,[32,39] and Lambert's cyclophane-bridged dyad.[35] These remain isolated examples with varying linkers and differing characterization precluding the systematic structure property relationships. Here, we report five pseudo-*para* substituted phenylalkyne PCPs featuring A–A, D–D, and D–A substituents and study their optical properties in solution and their electrical properties in the solid state.

gallium–indium (EGaIn)-based junctions have enabled the measurement of rectifying behavior across large areas in a single junction, providing a useful platform to bridge molecular and macroscopic device behavior.[22–24] Initial demonstrations of organic molecules displaying current rectification were inspired by the Aviram–Ratner model, which proposed donor–(σ-bridge)–acceptor motifs as molecular diodes.[25,26] In quick succession, Ashwell and co-workers reported that the R value could be improved when a donor–(π-bridge)–acceptor (D–π–A) system with large dipole moments, induced through zwitterionic charging.[28] Very few examples of molecular diodes based on a D–π–A structure have been demonstrated.[27–30] The model used to define rectification is based on the electronic asymmetry arising from the difference between the ionization energy of the donor and the electron affinity of the acceptor,[3,5,8,11] suggesting that the molecular dipole moment could be a good handle for tuning rectification behaviour.

Cedric Schaack was born and raised in Luxembourg. Cedric completed his PhD in Chemistry (2019) at ETH Zurich under the supervision of Francois Diederich. He was a postdoctoral researcher at Columbia University working with Professors Latha Venkataraman and Colin Nuckolls. Currently, Cedric is an assistant professor at the Wake Forest University. The Schaack lab's research focuses on the development of novel organic scaffolds that combine chirality

Cedric Schaack

with electronic properties. This work aims to engineer materials with new chiroptical properties for applications in organic electronics. In his free time, Cedric enjoys hiking in the nearby Appalachian Mountains and traveling across the US, embracing the natural beauty of North Carolina.

Aiming to establish quantitative structure–property relationships that compare both emissive behavior and rectification, we turned to the well-established PCP scaffold to probe how the molecular dipole impacts optoelectronic and rectification behavior. PCP is a structurally unique scaffold characterized by its rigid, non-planar π-system and through-space conjugation. The cofacial benzene rings of PCP are separated by a narrow ethylene bridge (~ 3 Å), allowing for significant intramolecular π–π interactions without requiring planarity. This spatial arrangement has been exploited extensively in organic electronics, most notably in OLEDs, where chiral PCP-based emitters have enabled high-performance TADF, circularly polarized luminescence (CPL), and color-pure emission (Fig. 1).[31–34] While donor–acceptor paracyclophanes have been previously explored by Bazan and Lambert,[35–37] these studies employed different linkers, substitution patterns, and molecular architectures, making direct comparisons impossible and precluding systematic structure–property relationships. Moreover, these studies focused primarily on optical properties, leaving the correlation between molecular dipole moments and solid-state rectification behavior unexplored. Our approach uses ethynyl linkers across five compounds, varying the terminal substituents in a controlled manner (D–D, A–A, and D–A). This systematic molecular study enables us to establish, for the first time, quantitative relationships between molecular asymmetry, electronic structure, and both photophysical and electrical performance in paracyclophanes. In contrast to well-studied linear π-systems, the influence of PCP's three-dimensional topology on solid-state charge transport remains underexplored.

In this work, we present five [2.2]paracyclophane-based donor–acceptor chromophores featuring electron-rich and electron-deficient substituents. These molecules were designed to explore how molecular asymmetry, dipole moment, and frontier molecular orbital (FMO) distributions affect both photophysical and electronic behavior. We characterize their solution-phase properties using UV-vis absorption and photoluminescence (PL) spectroscopy and probe their stimuli-responsive behavior *via* solvent titration studies

21760 | *J. Mater. Chem. C*, 2025, **13**, 21759–21767

This journal is © The Royal Society of Chemistry 2025

(solvatochromism) and aggregation-induced emission (AIE) experiments. Solid-state electrical properties are investigated using EGaIn-based junctions to measure current–voltage characteristics under forward and reverse bias. Collectively, these results establish PCP-based D–A systems as promising candidates for multifunctional organic electronic materials that combine tunable emission with directional charge transport.

Results and discussion

Our molecular design strategy centered on systematically functionalizing the [2.2]paracyclophane (PCP) scaffold with electronically distinct substituents to probe the influence of D–A interactions on photophysical and electronic behavior. To this end, we synthesized a family of symmetrically and asymmetrically substituted PCP derivatives bearing electron-donating (OMe), electron-withdrawing (CN), and weakly withdrawing (F) groups. Our five-compound series (compounds **1–5**) was designed to provide: (1) symmetric electron-poor (F–F **1**, CN–CN **3**) and electron-rich (OMe–OMe **2**) references with minimal dipole moments, (2) asymmetric D–A compounds (OMe-CN **4**, OMe-F **5**) with fixed dipole magnitudes, and (3) direct structure–property relationships for both photophysical and electrical behavior. We used ethyn-1,2-yl linkers to link the groups to the PCP core because they enable efficient synthesis and facilitate conjugation to the pendant aryl groups independently of bond rotations.[33,35,40]

The synthetic route begins with the preparation of 4,15-diethynyl[2.2]paracyclophane (**6**) according to established procedures.[41] Precursor **6** readily undergoes Sonogashira cross-coupling with aryl bromides under standard conditions to yield a mixture of monosubstituted intermediates, as well as the bis-substituted derivatives **1–3**. To prepare the D–A compounds, we found that sequential addition of acceptors, followed by donors, in a one pot setup allowed for the preparation of a mixture of D–D, A–A, and D–A compounds, something that was previously reported by Lambert and co-workers.[35] We thus employed this method to prepare OMe–CN **4** and OMe–F **5** directly from precursor **6** by introducing 4-bromoanisole and either 4-bromobenzonitrile or 4-bromofluorobenzene in equimolar amounts.

Single crystals of compounds F–F **1** and CN–CN **3** were obtained *via* vapor diffusion crystallization of pentane into dichloromethane solutions at 5 °C. These two compounds crystallize in a monoclinic crystal system with $P2_1/c$ space group (Fig. 2b and c). The structures show the typical rigidity and distortions inherent to PCP scaffolds while the substituent arene rings are co-planar with the PCP-phenyl framework.[42,43] There are weak intermolecular π–π interactions between neighboring [2.2]paracyclophanes, with a C···C distance of 3.496 Å and 3.330 Å for F–F **1** and CN–CN **3** respectively. CN–CN **3** displayed a slip-stacked conformation with a 33° interplanar angle between adjacent cyclophane phenyl groups. This angle increases to close to 90° in F–F **1**, a T-shaped π–π stacking interaction. Both of these geometries are indicative of favorable π–π interactions, which can result in intermolecular exciton coupling in addition to the through-space intramolecular communication typical of PCPs, and could explain the aggregation behavior observed in solution (*vide infra*).[44]

To investigate the electronic effects of donor and acceptor substitution on racemic PCPs **1–5**, we examined their steady-state UV-vis absorption and PL spectra (Fig. 3a and b). OMe–CN **4**, which features a donor–acceptor motif, exhibited a minor, red-shifted absorption profile compared to the bis-substituted control compounds **2** and **3**. This observation aligns well with reports that D–A PCPs exhibit only minor redshifts in absorption.[35–38] Time-dependent density functional theory (TD-DFT) calculations (ORCA 6.0.0, cam-B3LYP/def2-TZVP, 30 states)[45–48] indicate that low-energy excitations involve primarily the HOMO → LUMO transition, with additional contributions from nearby orbitals due to orbital mixing (Fig. 4 contains the Frontier molecular orbitals). Experimentally, PL spectra revealed a more striking difference: the emission wavelength of OMe–CN **4** ($\lambda_{max,em}$ = 433 nm) was dramatically red-shifted in comparison to all other compounds. This redshift was accompanied by an increased photoluminescence quantum yield (PLQY) from 1% in F–F **1** to 31% in OMe–CN **4**. Crucially, donor–acceptor dyad OMe–CN **4** displays similar PLQY in various solvents, which is significantly different than findings by Lambert (no fluorescence in D–A dyads) and Bazan (quenching of fluorescence in apolar solvents). We further characterized the time-resolved photoluminescence dynamics across our model series.[35,37]

This substantial increase in PLQY, along with the minimal spectral overlap between emission and absorption, and the red-shifted emission, support the formation of an ICT excited state, matching other reports of fluorescent PCPs.[37] Stabilization of this excited state, potentially accompanied by molecular reorganization that reduces non-radiative decay channels,
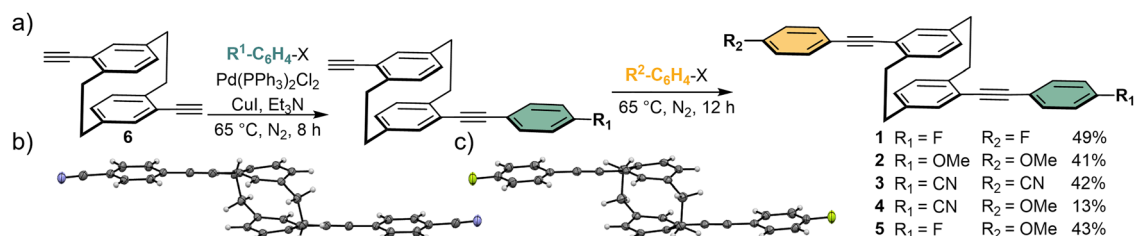

Fig. 2 (a) General synthetic scheme to afford compounds **1–5**, relying on sequential or parallel Sonogashira couplings to introduce various arene substituents onto the PCP core. (b) Single crystal structure of compound **3** and (c) compound **1** in the $P2_1/c$ space group. Ellipsoids are shown at the 50% probability level for both crystal structures.

Reaction scheme labels:

R^1-C$_6$H$_4$-X
Pd(PPh$_3$)$_2$Cl$_2$
CuI, Et$_3$N
65 °C, N$_2$, 8 h

R^2-C$_6$H$_4$-X
65 °C, N$_2$, 12 h

1 R$_1$ = F   R$_2$ = F   49%
2 R$_1$ = OMe R$_2$ = OMe 41%
3 R$_1$ = CN   R$_2$ = CN   42%
4 R$_1$ = CN   R$_2$ = OMe 13%
5 R$_1$ = F   R$_2$ = OMe 43%

This journal is © The Royal Society of Chemistry 2025

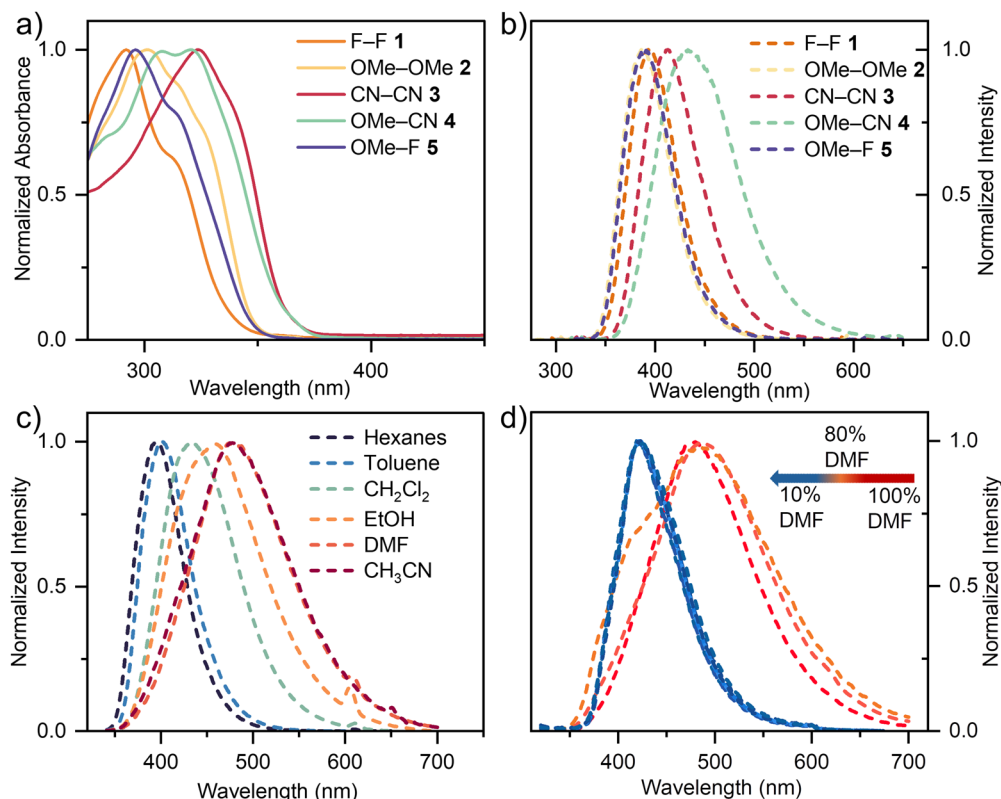*J. Mater. Chem. C*, 2025, **13**, 21759–21767 | **21761**

Fig. 3 (a) UV-vis absorption spectra (solid line, CH_2Cl_2, $c \sim 10^{-5}$ M) and (b) photoluminescence emission spectra (dashed line, $CHCl_3$, $c \sim 10^{-5}$ M) of F–F **1** (orange), OMe–OMe **2** (yellow), CN–CN **3** (red), OMe–CN **4** (cyan), and OMe–F **5** (purple); (c) photoluminescence spectra (dashed line, $CHCl_3$, $c \sim 10^{-5}$ M) of OMe–CN **4** in hexanes (black), toluene (blue), CH_2Cl_2 (cyan), ethanol (orange), N,N-dimethylformamide (DMF, red), and CH_3CN (burgundy). (d) Aggregated induced photoluminescence of OMe–CN **4** obtained by adding fractional volumes of H_2O into DMF.

likely contributes to the enhanced PLQY. In contrast, the OMe–OMe **2** and CN–CN **3** compounds exhibited only minor red-shifting relative to F–F **1**, which we attribute to modest shifts in their HOMO and LUMO levels induced by the electron-donating and electron-accepting moiety, respectively. As a result, their optical bandgaps remain largely unchanged. In asymmetric compounds such as OMe–CN **4**, however, the combination of a donor and acceptor leads to a narrowed bandgap due to both HOMO destabilization and LUMO stabilization.

FMO analysis reveals significant spatial separation of the HOMO and LUMO in OMe–CN **4**, consistent with ICT character: the HOMO is localized on the anisole-containing PCP half, while the LUMO is localized on the acceptor side (Fig. 4). This contrasts with symmetric compounds **1**–**3**, where both orbitals are delocalized across the molecular backbone due to the absence of a permanent dipole. Interestingly, in donor-rich OMe–F **5**, the HOMO remains localized on the electron-rich half, but the LUMO is fully delocalized, suggesting partial ICT character, though less pronounced than in OMe–CN **4**, likely due to the absence of a strong electron acceptor to localize the LUMO.

The interplay between spectral shifts and time-resolved photoluminescence dynamics across this series of molecular chromophores reveals a coherent narrative about how electronic structure governs excited-state behavior. The spectral
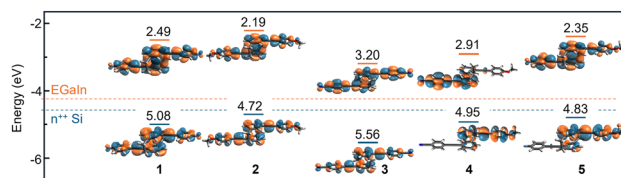

Fig. 4 Energy level alignment of PCP derivatives **1**–**5** with electrode materials. The work functions of n^{++}–Si (4.8 eV) and EGaIn (4.3 eV) are shown for comparison. HOMO (bottom) and LUMO (top) energies were obtained from DFT calculations (ORCA 6.0.0, PBE/def2-SVP) and are reported relative to vacuum. Frontier molecular orbitals are visualized at an isovalue of 0.03 e^- $Å^{-3}$, highlighting differences in orbital localization across symmetric and donor–acceptor substituted PCPs.

evolution is reflected in the decay kinetics shown in Fig. S40 in the SI: F–F **1**, with its blue-shifted emission, shows a dominant fast decay component, indicative of strong nonradiative quenching and limited stabilization of the excited state. OMe–OMe **2** and CN–CN **3** present more balanced biexponential profiles, suggesting a mixture of prompt and delayed relaxation pathways—likely arising from conformational flexibility and competing radiative and nonradiative channels. OMe–CN **4** stands apart, exhibiting both the largest red shift and the cleanest decay signature, with the two estimated lifetimes (τ_1 and τ_2) comparatively closely spaced and minimal residual structure. This points to a more rigid, electronically

21762 | J. Mater. Chem. C, 2025, **13**, 21759–21767

This journal is © The Royal Society of Chemistry 2025

delocalized excited state with fewer competing non-radiative pathways, resulting in a nearly monoexponential relaxation.

To further evaluate the presence of a highly polar push–pull charge-transfer state, we performed a solvatochromic study across solvents of varying polarity (Fig. 3c). While CN–CN **3** displayed modestly redshifted emission in polar solvents, compounds **1**, **2**, and **5** showed no solvent effects. Interestingly, OMe–CN **4** demonstrated significantly more pronounced solvatochromic behavior: its emission maximum shifted from 396 nm in hexanes to 474 nm in DMF, while the absorption spectrum remained largely unchanged. Interestingly, the shift in emission wavelength gives a good linear correlation to the solvent dielectric, but no correlation to solvent viscosity (see Fig. S19 in the SI). The large solvent-dependent red-shift, combined with minimal changes in absorption, supports the assignment of a CT excited state for OMe–CN **4**. This CT characteristic is further evidenced by the unusually large Stokes shift, which increased from 91 nm in hexanes to 166 nm in DMF, highlighting substantial excited-state reorganization. Similar observations were reported by Bartholomew et al.,[37] who described a ~ 100 nm red-shift in fluorescence wavelength when comparing hexane and chloroform solutions of D–A PCPs (Fig. 1). This finding is in line with expectations: a strong donor–acceptor character results in a dipolar excited state, which is more effectively stabilized by polar solvents, reducing the emission energy.

Given the varied emission behavior in solution, we next explored the influence of aggregation on photoluminescence by studying all five compounds in DMF–water mixtures of increasing water content. F–F **1** showed a modest red-shift (396 → 404 nm) and increased PL intensity upon reaching a 1:1 DMF:water ratio. In molecular aggregates, spectral shifts can be rationalized in terms of exciton coupling models.[49–52] A red shift in emission is generally associated with J-type aggregation, in which head-to-tail molecular packing lowers the energy of the emissive exciton state, which is often accompanied by increasing radiative rates. Conversely, a blue shift is indicative of H-type aggregation, where face-to-face packing raises the energy of the emissive state, which can suppress radiative decay. In our systems, the modest red shift and PL intensity increase observed for F–F **1** is consistent with J-aggregation, whereas the hypsochromic shift (486 → 421 nm) starting at 30% water content (Fig. 3d) seen for OMe–CN **4** in DMF–water mixtures supports H-type aggregation. Conversely, OMe–OMe **2** and CN–CN **3** exhibited only minor red- and blue-shifting respectively, with rapid fluorescence quenching upon aggregation. Photographic images and photoluminescence spectra for all compounds can be found in the SI (Fig. S13-S18).

These solution-phase studies highlight the unique optoelectronic behavior of OMe–CN **4**, including a stabilized charge-transfer excited state and robust photoluminescence across diverse environments. We next sought to evaluate whether the dipole moment from this rigid scaffold would correlate to charge transport in a solid-state device configuration. A molecular diode characterization was conducted to observe the effect of the inherent molecular dipole on current rectification.

In previous studies, rectification ratios $\left(R = \frac{|J_{+V}|}{|J_{-V}|} \right)$ have been shown to correlate with the molecular dipole,[53] and vary widely depending on measurement conditions, from $R < 10$ in disordered or damaged thin films to $R > 1000$ in densely packed self-assembled monolayers (SAMs). Most established organic rectifiers display R values ~ 30–100,[54,55] and contain flexible sp^3 chains with conformationally dependent dipole moments, requiring highly dense and ordered surface assembly to achieve sufficient molecular orientation. Even minor defects in these monolayers result in dramatic current leakage and corresponding collapse of rectification ratios, highlighting the fragility of this approach.[56]

The PCP scaffold offers several distinct advantages over conventional linear rectifiers: (1) the rigid, three-dimensional structure prevents conformational disorder that typically reduces rectification in flexible molecules; (2) the through-space conjugation provides an additional electronic coupling pathway absent in traditional rectifiers; and (3) supramolecular stacking, as evidenced from the tendency to crystallize, can contribute to making the PCP layer a high dielectric semiconductor, which could in turn be beneficial for developing thin film diodes. Thus, we evaluated the electrical properties of **1–5** using a vertical metal–semiconductor–metal architecture (Fig. S33). Detailed fabrication procedures are provided in the Methods section of SI. Briefly, thin films of each cyclophane were prepared by spin coating their toluene solutions onto cleaned, highly doped n^{++}–Si substrates. Atomic force microscopy (AFM) was used to confirm film thicknesses and revealed that all samples formed a packed but discontinuous film (Fig. S28-S32), likely due to the strong crystallization tendencies of these molecules. This is consistent with their aggregation behavior in solution and their ability to grow single crystals suitable for SC-XRD.

To ensure reproducible, non-destructive electrical contact, we employed EGaIn as the top electrode. This soft metal is widely used in molecular rectifier studies due to its conformal contact and minimal damage to fragile organic films.[57] In addition, EGaIn electrodes form contacts over mm^2-scale areas, allowing for measurement of spatially averaged charge transport across the heterogeneous film, rather than being dominated by local defects or conductive hotspots. The high superficial tension of EGaIn ensures a sufficient contact area for result reproducibility.

Upon biasing EGaIn relative to the Si bottom electrode, we recorded current–voltage (*I–V*) characteristics for each molecule and plotted the thickness-normalized currents for comparison (Fig. 5a). Based on DFT calculations and redox potentials obtained *via* cyclic voltammetry (Fig. S20-S27), we infer that hole-only transport dominates in these devices (Fig. 4). Among the symmetric cyclophanes, both F–F **1** and OMe–OMe **2** exhibited conductance values four orders of magnitude higher than CN–CN **3**, attributable to a lower injection barrier at the Si interface resulting from their higher-lying HOMO levels. As expected, the D–A compound OMe–CN **4** also exhibited high
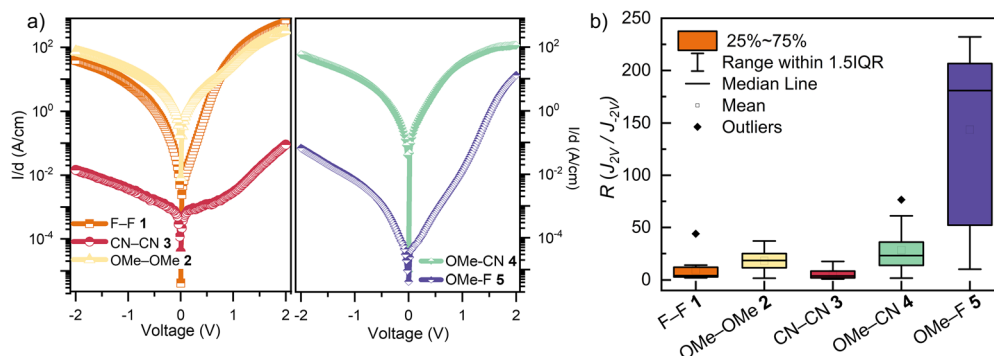
This journal is © The Royal Society of Chemistry 2025

J. Mater. Chem. C, 2025, **13**, 21759–21767 | **21763**

Fig. 5 (a) Current–voltage (I–V) characteristics of EGaIn junctions incorporating compounds **1**–**5** measured on n^{++} Si substrates, showing the thickness-normalized current $|I/d|$ (A cm^{-1}) *versus* applied bias. Data are color-coded by compound: F–F **1** (orange), OMe–OMe **2** (yellow), CN–CN **3** (red), OMe–CN **4** (cyan), and OMe–F **5** (purple). (b) Corresponding rectification ratios R calculated as $|J_{(+2V)}/J_{(-2V)}|$ for each compound reveal strong dipole-dependent current modulation in the D–A systems.

conductance, likely due to a reduced effective injection barrier and a HOMO level comparable to OMe–OMe **2**.

Interestingly, this trend did not hold uniformly across the two D–A systems. While F–F **1** and OMe–OMe **2** displayed high and nearly equivalent conductance, their asymmetric counterpart, OMe–F **5** exhibited conductance suppressed by four orders of magnitude under negative bias. Despite this suppression, OMe–F **5** showed pronounced current rectification, with a rectification ratio R reaching as high as 200 at $|2\,V|$ (Fig. 5b). The exceptional rectification in OMe–F **5**, despite its lower conductance, suggests that rectification and conductance are independently tunable in PCP systems, a valuable design principle for molecular electronics where both high on-currents and high on/off ratios are desired. While some reported rectifiers have achieved higher rectification ratios through precise molecular orientation in SAMs and the incorporation of redox-active metal centers (up to $R \sim 1 \times 10^3$),[18,58–60] our approach demonstrates a new molecular scaffold for charge transport. We achieve $R \sim 200$ in solution-processed, amorphous films without requiring the stringent organizational control of SAMs, dramatically simplifying device fabrication and robustness compared to flexible molecular rectifiers, where specific conformations must be maintained through careful assembly.[55,61–63] Remarkably, this degree of rectification was consistently reproduced across 45 independent measurements.[57] These results underscore the value of the EGaIn method, which samples large contact areas and captures intrinsic molecular behavior beyond local disorder.

To further evaluate the influence of film morphology, we performed I–V sweeps across multiple spatial locations and devices. As shown in Fig. S34–S38, we observed a broad distribution in current values, reflecting the order dependence of device performance. Notably, the OMe–F **5** compound (Fig. S38) exhibited a bimodal distribution in its average rectification ratio (R_{avg}) centered around $R_{\mathrm{avg}} \approx 20$ and $R_{\mathrm{avg}} \approx 200$, each based on 45 measurements. This likely reflects two distinct molecular orientations or packing motifs in the film. Based on the direct correlation of the molecular dipole to the current rectification, we believe that higher rectification might be achievable through controlled molecular alignment, such as in self-assembled monolayers, which is currently under investigation in our laboratory. OMe–CN **4** PCP also

demonstrated enhanced rectification ($R_{\mathrm{avg}} \approx 35$) relative to OMe–OMe **2** ($R_{\mathrm{avg}} \approx 15$) and CN–CN **3** ($R_{\mathrm{avg}} \approx 5$), with some individual devices exhibiting rectification as high as $R \approx 75$. These results collectively support the hypothesis that molecular asymmetry and dipole moment are key factors in achieving diode behavior in organic systems.

Even when accounting for interface variability, rectification ratios showed a strong correlation with molecular dipole moments (Fig. 5b). While compounds **1**–**3**, due to their symmetric substitution, exhibit only small dipoles, the D–A cyclophanes OMe–CN **4** and OMe–F **5** possess significant dipole vectors directed from donor to acceptor. This positive correlation aligns with prior reports on molecular rectifiers, where large dipole moments produce internal electric fields that facilitate charge injection under forward bias and suppress it under reverse bias. Although the films studied here are not monolayers, the high R_{avg} in the dipolar OMe–F **5** system illustrates the relevance of electronic asymmetry in charge transport through substituted paracyclophanes. Ongoing studies aim to further elucidate this structure–function relationship.

Conclusion

This study demonstrates that rationally substituted pseudo-*para* [2.2]paracyclophanes function as versatile molecular materials, exhibiting both pronounced charge-transfer photophysics and diode-like electrical behavior. By systematically tuning substituent identity and symmetry, we discovered structure–property relationships that govern emission, aggregation behavior, and solid-state rectification. In solution, the D–A PCP **4** displays a large Stokes shift, solvent-dependent emission, and robust photoluminescence in aggregated states, indicative of stabilized charge-transfer excited states. In thin films, these D–A compounds exhibit current rectification with R up to 200, remarkable for solution-processed films measured across millimeter-scale junctions. This performance, achieved without molecular ordering or surface engineering, highlights the robustness of the PCP scaffold's rigid D–π–A architecture. These findings underscore the potential of push–pull PCPs as

dual-mode optoelectronic materials that bridge emissive and electronic function. Ongoing studies in our lab are focused on producing self-assembled monolayers of various D–A substituted paracyclophanes to investigate their diode properties in more ordered and controlled interfaces. Together, these results lay the groundwork for incorporating [2.2]paracyclophane-based motifs into advanced molecular electronic devices, including rectifiers, sensors, and light-emitting diodes, and highlight the broader utility of through-space conjugated platforms in next-generation organic electronics.

Conflicts of interest

There are no conflicts to declare.

Data availability

The data supporting this article have been included as part of the supplementary information (SI). Supplementary information contains additional data and experimental details, including materials and instrumentation, synthetic procedures and characterization, UV-Vis, photoluminescence data, cyclic voltammetry, NMR traces, TRPL data, and computational results. See DOI: https://doi.org/10.1039/d5tc02049b.

Raw data supporting the findings of this study are available from the corresponding author Cedric Schaack upon reasonable request.

CCDC 2453599 and 2453610 contain the supplementary crystallographic data for this paper.[64a,b]

Acknowledgements

References

1 H. Chen and F. J. Stoddart, From Molecular to Supramolecular Electronics, *Nat. Rev. Mater.*, 2021, **6**(9), 804–828, DOI: 10.1038/s41578-021-00302-2.

2 C. J. Kousseff, R. Halaksa, Z. S. Parr and C. B. Nielsen, Mixed Ionic and Electronic Conduction in Small-Molecule Semiconductors, *Chem. Rev.*, 2022, **122**(4), 4397–4419, DOI: 10.1021/acs.chemrev.1c00314.

3 S. Ma, S. Du, G. Pan, S. Dai, B. Xu and W. Tian, Organic Molecular Aggregates: From Aggregation Structure to Emission Property, *Aggregate*, 2021, **2**(4), e96, DOI: 10.1002/agt2.96.

4 S. R. Forrest, The Path to Ubiquitous and Low-Cost Organic Electronic Appliances on Plastic, *Nature*, 2004, **428**(6986), 911–918, DOI: 10.1038/nature02498.

5 J. Zhao, L. Jiao, L. Kinziabulatova, T. J. Williams, R. M. Gracia, A. Gartner, T. A. Stich, W. Ding, M. Son and C. Schaack, Allenes as Stimuli-Responsive Chromophores for Visible to Near-Infrared Optical Modulation, *J. Am. Chem. Soc.*, 2025, **147**(36), 32710–32716, DOI: 10.1021/jacs.5c08383.

6 S. J. Brown, J. Zhao, E. Forehand, L. Dobrzycki, R. Roy, A. M. M. Hasan, W. Ding, C. Schaack and A. M. Evans, Readily Accessible, Versatile, and Adaptive Biaxially Chiral Chromophores, *J. Am. Chem. Soc.*, 2025, **147**(4), 3769–3775, DOI: 10.1021/jacs.4c16566.

7 M. Makala, M. Barłóg, D. Dremann, S. Attar, E. G. Fernández, M. Al-Hashimi and O. D. Jurchescu, High-Performance n-Type Polymer Field-Effect Transistors with Exceptional Stability, *J. Mater. Chem. C*, 2024, **12**(42), 17089–17098, DOI: 10.1039/D4TC03294B.

8 Y.-J. Cheng, S.-H. Yang and C.-S. Hsu, Synthesis of Conjugated Polymers for Organic Solar Cell Applications, *Chem. Rev.*, 2009, **109**(11), 5868–5923, DOI: 10.1021/cr900182s.

9 I. Park, C. Kim, R. Kim, N. Li, J. Lee, O. K. Kwon, B. Choi, T. N. Ng and D.-S. Leem, High Performance Shortwave Infrared Organic Photodetectors Adopting Thiadiazole Quinoxaline-Based Copolymers, *Adv. Opt. Mater.*, 2022, **10**(19), 2200747, DOI: 10.1002/adom.202200747.

10 S. Ko, R. Mondal, C. Risko, J. K. Lee, S. Hong, M. D. McGehee, J.-L. Brédas and Z. Bao, Tuning the Optoelectronic Properties of Vinylene-Linked Donor−Acceptor Copolymers for Organic Photovoltaics, *Macromolecules*, 2010, **43**(16), 6685–6698, DOI: 10.1021/ma101088f.

11 T.-T. Bui, F. Goubard, M. Ibrahim-Ouali, D. Gigmes and F. Dumur, Recent Advances on Organic Blue Thermally Activated Delayed Fluorescence (TADF) Emitters for Organic Light-Emitting Diodes (OLEDs, *Beilstein J. Org. Chem.*, 2018, **14**, 282–308, DOI: 10.3762/bjoc.14.18.

12 B. Madushani, M. Mamada, K. Goushi, T. B. Nguyen, H. Nakanotani, H. Kaji and C. Adachi, Multiple Donor–Acceptor Design for Highly Luminescent and Stable Thermally Activated Delayed Fluorescence Emitters, *Sci. Rep.*, 2023, **13**(1), 7644, DOI: 10.1038/s41598-023-34623-9.

13 B. Yang, S. Yan, Y. Zhang, F. Feng and W. Huang, Stimuli-Responsive Luminescence from Polar Cyano/Isocyano-Derived Luminophores via Structural Tailoring and Self-Assembly, *Dalton Trans.*, 2024, **53**(12), 5320–5341, DOI: 10.1039/D3DT04049F.

14 Y. Yu, N. Qiang, Z. Liu, M. Lu, Y. Shen, J. Zou, J. Yang and G. Liu, Multi-Stimuli-Responsive Fluorescent Molecule with AIE and TICT Properties Based on 1,8-Naphthalimide, *Nanomaterials*, 2024, **14**(15), 1255, DOI: 10.3390/nano14151255.

15 H. Tsujimoto, D.-G. Ha, G. Markopoulos, H. S. Chae, M. A. Baldo and T. M. Swager, Thermally Activated Delayed Fluorescence and Aggregation Induced Emission with Through-Space Charge Transfer, *J. Am. Chem. Soc.*, 2017, **139**(13), 4894–4900, DOI: 10.1021/jacs.7b00873.

16 V. Kachwal and J.-C. Tan, Stimuli-Responsive Electrospun Fluorescent Fibers Augmented with Aggregation-Induced Emission (AIE) for Smart Applications, *Adv. Sci.*, 2023, **10**(1), 2204848, DOI: 10.1002/advs.202204848.

17 Y. Guo, C. Yang, S. Zhou, K. N. Houk and X. Guo, A Robust Single-Molecule Diode with High Rectification Ratio and

This journal is © The Royal Society of Chemistry 2025

J. Mater. Chem. C, 2025, **13**, 21759–21767 | **21765**

Integrability, *J. Am. Chem. Soc.*, 2025, **147**(20), 16972–16981, DOI: **10.1021/jacs.5c00566**.

18 R. P. Sullivan, J. T. Morningstar, E. Castellanos-Trejo, R. W. Bradford, Y. J. Hofstetter, Y. Vaynzof, M. E. Welker and O. D. Jurchescu, Intermolecular Charge Transfer Enhances the Performance of Molecular Rectifiers, *Sci. Adv.*, 2022, **8**(31), eabq7224, DOI: **10.1126/sciadv.abq7224**.

19 T. He, M. Stolte, Y. Wang, R. Renner, P. P. Ruden, F. Würthner and C. D. Frisbie, Site-Specific Chemical Doping Reveals Electron Atmospheres at the Surfaces of Organic Semiconductor Crystals, *Nat. Mater.*, 2021, **20**(11), 1532–1538, DOI: **10.1038/s41563-021-01079-z**.

20 H. Zhang, J. Li, C. Yang and X. Guo, Single-Molecule Functional Chips: Unveiling the Full Potential of Molecular Electronics and Optoelectronics, *Acc. Mater. Res.*, 2024, **5**(8), 971–986, DOI: **10.1021/accountsmr.4c00125**.

21 B. Capozzi, J. Xia, O. Adak, E. J. Dell, Z.-F. Liu, J. C. Taylor, J. B. Neaton, L. M. Campos and L. Venkataraman, Single-Molecule Diodes with High Rectification Ratios through Environmental Control, *Nat. Nanotechnol.*, 2015, **10**(6), 522–527, DOI: **10.1038/nnano.2015.97**.

22 H. Wang, F. Hu, A. Adijiang, R. Emusani, J. Zhang, Q. Hu, X. Guo, T. Lee, L. Chen and D. Xiang, Gating the Rectifying Direction of Tunneling Current through Single-Molecule Junctions, *J. Am. Chem. Soc.*, 2024, **146**(51), 35347–35355, DOI: **10.1021/jacs.4c13773**.

23 M. Carlotti, M. Degen, Y. Zhang and R. C. Chiechi, Pronounced Environmental Effects on Injection Currents in EGaIn Tunneling Junctions Comprising Self-Assembled Monolayers, *J. Phys. Chem. C*, 2016, **120**(36), 20437–20445, DOI: **10.1021/acs.jpcc.6b07089**.

24 X. Xu, C. Gao, R. Emusani, C. Jia and D. Xiang, Toward Practical Single-Molecule/Atom Switches, *Adv. Sci.*, 2024, **11**(29), 2400877, DOI: **10.1002/advs.202400877**.

25 A. Aviram and M. A. Ratner, Molecular Rectifiers, *Chem. Phys. Lett.*, 1974, **29**(2), 277–283, DOI: **10.1016/0009-2614(74)85031-1**.

26 N. J. Geddes, J. R. Sambles, D. J. Jarvis, W. G. Parker and D. J. Sandman, The Electrical Properties of Metal-Sandwiched Langmuir–Blodgett Multilayers and Monolayers of a Redox-Active Organic Molecular Compound, *J. Appl. Phys.*, 1992, **71**(2), 756–768, DOI: **10.1063/1.351340**.

27 A. S. Martin, J. R. Sambles and G. J. Ashwell, Molecular Rectifier, *Phys. Rev. Lett.*, 1993, **70**(2), 218–221, DOI: **10.1103/PhysRevLett.70.218**.

28 G. J. Ashwell, J. R. Sambles, A. S. Martin, W. G. Parker and M. Szablewski, Rectifying Characteristics of Mg|(C16H33-Q3CNQ LB Film)|Pt Structures, *J. Chem. Soc., Chem. Commun.*, 1990, **19**, 1374–1376, DOI: **10.1039/C39900001374**.

29 G. J. Ashwell, A. Chwialkowska and L. R. H. High, Au-S-CH2-Q3CNQ: Self-Assembled Monolayers for Molecular Rectification, *J. Mater. Chem.*, 2004, **14**(15), 2389–2394, DOI: **10.1039/B403942D**.

30 G. J. Ashwell, A. Mohib and J. R. Miller, Induced Rectification from Self-Assembled Monolayers of Sterically Hindered π-Bridged Chromophores, *J. Mater. Chem.*, 2005, **15**(11), 1160–1166, DOI: **10.1039/B417880G**.

31 M.-Y. Zhang, Z.-Y. Li, B. Lu, Y. Wang, Y.-D. Ma and C.-H. Zhao, Solid-State Emissive Triarylborane-Based [2.2]Paracyclophanes Displaying Circularly Polarized Luminescence and Thermally Activated Delayed Fluorescence, *Org. Lett.*, 2018, **20**(21), 6868–6871, DOI: **10.1021/acs.orglett.8b02995**.

32 E. Spuling, N. Sharma, W. I. D. Samuel, E. Zysman-Colman and S. Bräse, (Deep) Blue through-Space Conjugated TADF Emitters Based on [2.2]Paracyclophanes, *Chem. Commun.*, 2018, **54**(67), 9278–9281, DOI: **10.1039/C8CC04594A**.

33 M. Gon, Y. Morisaki and Y. Chujo, Optically Active Cyclic Compounds Based on Planar Chiral [2.2]Paracyclophane: Extension of the Conjugated Systems and Chiroptical Properties, *J. Mater. Chem. C*, 2015, **3**(3), 521–529, DOI: **10.1039/C4TC02339K**.

34 Z. Hassan, E. Spuling, D. M. Knoll and S. Bräse, Regioselective Functionalization of [2.2]Paracyclophanes: Recent Synthetic Progress and Perspectives, *Angew. Chem., Int. Ed.*, 2020, **59**(6), 2156–2170, DOI: **10.1002/anie.201904863**.

35 C. Kaiser, A. Schmiedel, M. Holzapfel and C. Lambert, Long-Lived Singlet and Triplet Charge Separated States in Small Cyclophane-Bridged Triarylamine–Naphthalene Diimide Dyads, *J. Phys. Chem. C*, 2012, **116**(29), 15265–15280, DOI: **10.1021/jp304391x**.

36 J. W. Hong, H. Y. Woo, B. Liu and G. C. Bazan, Solvatochromism of Distyrylbenzene Pairs Bound Together by [2.2]Paracyclophane: Evidence for a Polarizable "Through-Space" Delocalized State, *J. Am. Chem. Soc.*, 2005, **127**(20), 7435–7443, DOI: **10.1021/ja044326**.

37 G. P. Bartholomew and G. C. Bazan, Synthesis, Characterization, and Spectroscopy of 4,7,12,15-[2.2]Paracyclophane Containing Donor and Acceptor Groups: Impact of Substitution Patterns on Through-Space Charge Transfer, *J. Am. Chem. Soc.*, 2002, **124**(18), 5183–5196, DOI: **10.1021/ja0121383**.

38 J. Zyss, I. Ledoux, S. Volkov, V. Chernyak, S. Mukamel, G. P. Bartholomew and G. C. Bazan, Through-Space Charge Transfer and Nonlinear Optical Properties of Substituted Paracyclophane, *J. Am. Chem. Soc.*, 2000, **122**(48), 11956–11962, DOI: **10.1021/ja0022526**.

39 X. Liang, T.-T. Liu, Z.-P. Yan, Y. Zhou, J. Su, X.-F. Luo, Z.-G. Wu, Y. Wang, Y.-X. Zheng and J.-L. Zuo, Organic Room-Temperature Phosphorescence with Strong Circularly Polarized Luminescence Based on Paracyclophanes, *Angew. Chem., Int. Ed.*, 2019, **58**(48), 17220–17225, DOI: **10.1002/anie.201909076**.

40 Y. Morisaki and Y. Chujo, Through-Space Conjugated Polymers Based on Cyclophanes, *Angew. Chem., Int. Ed.*, 2006, **45**(39), 6430–6437, DOI: **10.1002/anie.200600752**.

41 L. Bondarenko, I. Dix and H. Hinrichs, Hopf, H. Cyclophanes. Part LII: Ethynyl[2.2]Paracyclophanes - New Building Blocks for Molecular Scaffolding, *Synthesis*, 2004, 2751–2759, DOI: **10.1055/s-2004-834872**.

42 H. Hope, J. Bernstein and K. N. Trueblood, The Crystal and Molecular Structure of 1,1,2,2,9,9,10,10-Octafluoro-[2,2]Paracyclophane and a Reinvestigation of the Structure

21766 | *J. Mater. Chem. C*, 2025, **13**, 21759–21767

This journal is © The Royal Society of Chemistry 2025

of [2,2]Paracyclophane, *Acta Crystallogr., Sect. B*, 1972, **28**(6), 1733–1743, DOI: **10.1107/S0567740872004947**.

43 H. Wolf, D. Leusser, M. R. V. Jørgensen, R. Herbst-Irmer, Y.-S. Chen, E.-W. Scheidt, W. Scherer, B. B. Iversen and D. Stalke, Phase Transition of [2,2]-Paracyclophane – An End to an Apparently Endless Story, *Chem. – Eur. J.*, 2014, **20**(23), 7048–7053, DOI: **10.1002/chem.201304972**.

44 C. R. Martinez and B. L. Iverson, Rethinking the Term "Pi-Stacking, *Chem. Sci.*, 2012, **3**(7), 2191, DOI: **10.1039/c2sc20045g**.

45 F. Neese, An Improvement of the Resolution of the Identity Approximation for the Formation of the Coulomb Matrix, *J. Comput. Chem.*, 2003, **24**(14), 1740–1747, DOI: **10.1002/jcc.10318**.

46 F. Neese and G. Olbrich, Efficient Use of the Resolution of the Identity Approximation in Time-Dependent Density Functional Calculations with Hybrid Density Functionals, *Chem. Phys. Lett.*, 2002, **362**(1), 170–178, DOI: **10.1016/S0009-2614(02)01053-9**.

47 F. Neese, The SHARK Integral Generation and Digestion System, *J. Comput. Chem.*, 2023, **44**(3), 381–396, DOI: **10.1002/jcc.26942**.

48 F. Neese, Software Update: The ORCA Program System---Version 5.0, *Wiley Interdiscip. Rev.: Comput. Mol. Sci.*, 2022, **12**(5), e1606, DOI: **10.1002/wcms.1606**.

49 J. Mei, Y. Hong, J. W. Y. Lam, A. Qin, Y. Tang and B. Z. Tang, Aggregation-Induced Emission: The Whole Is More Brilliant than the Parts, *Adv. Mater.*, 2014, **26**(31), 5429–5479, DOI: **10.1002/adma.201401356**.

50 Y. Hong, J. W. Y. Lam and B. Z. Tang, Aggregation-Induced Emission, *Chem. Soc. Rev.*, 2011, **40**(11), 5361–5388, DOI: **10.1039/C1CS15113D**.

51 J. Mei, N. L. C. Leung, R. T. K. Kwok, J. W. Y. Lam and B. Z. Tang, Aggregation-Induced Emission: Together We Shine, United We Soar, *Chem. Rev.*, 2015, **115**(21), 11718–11940, DOI: **10.1021/acs.chemrev.5b00263**.

52 F. C. Spano, The Spectral Signatures of Frenkel Polarons in H- and J-Aggregates, *Acc. Chem. Res.*, 2010, **43**(3), 429–439, DOI: **10.1021/ar900233v**.

53 Z. A. Lamport, A. D. Broadnax, D. Harrison, K. J. Barth, L. Mendenhall, C. T. Hamilton, M. Guthold, T. Thonhauser, M. E. Welker and O. D. Jurchescu, Fluorinated Benzalkylsilane Molecular Rectifiers, *Sci. Rep.*, 2016, **6**(1), 38092, DOI: **10.1038/srep38092**.

54 M. Baghbanzadeh, L. Belding, L. Yuan, J. Park, M. H. Al-Sayah, C. M. Bowers and G. M. Whitesides, Dipole-Induced Rectification Across Ag^{TS}/SAM//Ga$_2$ O$_3$/EGaIn Junctions, *J. Am. Chem. Soc.*, 2019, **141**(22), 8969–8980, DOI: **10.1021/jacs.9b02891**.

55 M. Li, B. Tu, B. Cui, X. Zhao, L. Yang, Q. Fang, Y. Yan and B. A. Grzybowski, Efficient and Long-Lasting Current Rectification by Laminated Yet Separated, Oppositely Charged Monolayers, *ACS Appl. Electron. Mater.*, 2019, **1**(11), 2295–2300, DOI: **10.1021/acsaelm.9b00482**.

56 N. Nerngchamnong, L. Yuan, D.-C. Qi, J. Li, D. Thompson and C. A. Nijhuis, The Role of van der Waals Forces in the Performance of Molecular Diodes, *Nat. Nanotechnol.*, 2013, **8**(2), 113–118, DOI: **10.1038/nnano.2012.238**.

57 R. C. Chiechi, E. A. Weiss, M. D. Dickey and G. M. Whitesides, Eutectic Gallium–Indium (EGaIn): A Moldable Liquid Metal for Electrical Characterization of Self-Assembled Monolayers, *Angew. Chem., Int. Ed.*, 2008, **47**(1), 142–144, DOI: **10.1002/anie.200703642**.

58 K. Garg, C. Majumder, S. K. Nayak, D. K. Aswal, S. K. Gupta and S. Chattopadhyay, Silicon-Pyrene/Perylene Hybrids as Molecular Rectifiers, *Phys. Chem. Chem. Phys.*, 2015, **17**(3), 1891–1899, DOI: **10.1039/C4CP04044A**.

59 X. Chen, M. Roemer, L. Yuan, W. Du, D. Thompson, E. del Barco and C. A. Nijhuis, Molecular Diodes with Rectification Ratios Exceeding 105 Driven by Electrostatic Interactions, *Nat. Nanotechnol.*, 2017, **12**(8), 797–803, DOI: **10.1038/nnano.2017.110**.

60 W. F. Reus, M. M. Thuo, N. D. Shapiro, C. A. Nijhuis and G. M. Whitesides, The SAM, Not the Electrodes, Dominates Charge Transport in Metal-Monolayer//Ga$_2$ O$_3$/Gallium–Indium Eutectic Junctions, *ACS Nano*, 2012, **6**(6), 4806–4822, DOI: **10.1021/nn205089u**.

61 L. Yuan, R. Breuer, L. Jiang, M. Schmittel and C. A. Nijhuis, A Molecular Diode with a Statistically Robust Rectification Ratio of Three Orders of Magnitude, *Nano Lett.*, 2015, **15**(8), 5506–5512, DOI: **10.1021/acs.nanolett.5b02014**.

62 L. Yuan, N. Nerngchamnong, L. Cao, H. Hamoudi, E. del Barco, M. Roemer, R. K. Sriramula, D. Thompson and C. A. Nijhuis, Controlling the Direction of Rectification in a Molecular Diode, *Nat. Commun.*, 2015, **6**(1), 6324, DOI: **10.1038/ncomms7324**.

63 Z. A. Lamport, A. D. Broadnax, B. Scharmann, R. W. I. Bradford, A. DelaCourt, N. Meyer, H. Li, S. M. Geyer, T. Thonhauser, M. E. Welker and O. D. Jurchescu, Molecular Rectifiers on Silicon: High Performance by Enhancing Top-Electrode/Molecule Coupling, *ACS Appl. Mater. Interfaces*, 2019, **11**(20), 18564–18570, DOI: **10.1021/acsami.9b02315**.

64 (*a*) CCDC 2453599: Experimental Crystal Structure Determination, 2025, DOI: **10.5517/ccdc.csd.cc2nc5cl**; (*b*) CCDC 2453610: Experimental Crystal Structure Determination, 2025, DOI: **10.5517/ccdc.csd.cc2nc5qy**.

This journal is © The Royal Society of Chemistry 2025

J. Mater. Chem. C, 2025, **13**, 21759–21767 | **21767**